Editors' Suggestion | Featured in Physics

Single-Shot Readout of Multiple Donor Electron Spins with a Gate-Based Sensor

M.R. Hogg,[1,†] P. Pakkiam,[1,‡] S.K. Gorman,[1,2] A.V. Timofeev,[1] Y. Chung,[1,2] G.K. Gulati,[1,2] M.G. House,[1,2,§] and M.Y. Simmons[1,2,*]

[1] *Australian Research Council Centre of Excellence for Quantum Computation and Communication Technology, School of Physics, University of New South Wales, Sydney, NSW 2052, Australia*

[2] *Silicon Quantum Computing, Sydney, NSW 2052, Australia*

(Received 19 October 2021; revised 19 August 2022; accepted 4 January 2023; published 23 February 2023)

Proposals for large-scale semiconductor spin-based quantum computers require high-fidelity single-shot qubit readout to perform error correction and read out qubit registers at the end of a computation. However, as devices scale to larger qubit numbers integrating readout sensors into densely packed qubit chips is a critical challenge. Two promising approaches are minimizing the footprint of the sensors, and extending the range of each sensor to read more qubits. Here we show high-fidelity single-shot electron spin readout using a nanoscale single-lead quantum dot (SLQD) sensor that is both compact and capable of reading multiple qubits. Our gate-based SLQD sensor is deployed in an all-epitaxial silicon donor spin-qubit device, and we demonstrate single-shot readout of three ^{31}P donor quantum dot electron spins with a maximum fidelity of 95%. Importantly, in our device the quantum dot confinement potentials are provided inherently by the donors, removing the need for additional metallic confinement gates and resulting in strong capacitive interactions between sensor and donor quantum dots. Our results are consistent with a $1/d^{1.4}$ scaling of the capacitive coupling between sensor and ^{31}P dots (where d is the sensor-dot distance), compared to $1/d^{2.5-3.0}$ in gate-defined quantum dot devices. Due to the small qubit size and strong capacitive interactions in all-epitaxial donor devices, we estimate a single sensor can achieve single-shot readout of approximately 15 qubits in a linear array, compared to 3–4 qubits for a similar sensor in a gate-defined quantum dot device. Our results highlight the potential for spin-qubit devices with significantly reduced sensor densities.

DOI: 10.1103/PRXQuantum.4.010319

I. INTRODUCTION

High-fidelity single-shot spin readout is an essential requirement for large-scale spin-based quantum computing proposals [1,2]. In spin-qubit devices readout has most commonly been performed by mapping the spin state onto a charge state, which can then be detected using a nearby charge sensor [3,4]. The most sensitive charge sensors to date are radio-frequency single-electron transistors (rf SETs), which have demonstrated integration times for a SNR ratio of 1 of $\tau_{\mathrm{min}} = 0.62$ ns [5] (we use τ_{min} to directly compare sensor performance between experiments, see Section 1 within the Supplemental Material [6]). However rf SETs require at least three gate leads to operate, a significant space allocation on the qubit chip as devices scale to larger qubit numbers. In contrast gate-based (or dispersive) sensors integrate qubit readout capability into the existing leads used for qubit control, allowing spin measurements without additional proximal charge sensors [7–10]. Single-shot readout using dispersive sensors has recently been demonstrated [11–15], however these results relied on Pauli blockade between two spins for readout, requiring an additional quantum dot (with associated control leads) for spin detection. Furthermore, in each case readout of only a single qubit was achieved. Dispersive sensors probing interdot transitions (referred to here as "direct dispersive" sensors) can also generate only signal at an interdot charge transition, a small window in gate space. Experiments to date have thus often used a secondary multilead charge sensor for device characterization [11,12].

The SLQD is a gate-based sensor that combines the benefits of rf SETs and direct dispersive sensors [16]. In contrast to the rf SET, the SLQD requires only one electron

*Corresponding author. michelle.simmons@unsw.edu.au

†Present address: Department of Physics, The University of Basel, 4056 Basel, Switzerland.

‡Present address: School of Mathematics and Physics, The University of Queensland, 4067 Brisbane, Australia.

§Present address: PsiQuantum Ltd, 94304 Palo Alto, United States.

reservoir (making it more suited to integration with large-scale qubit arrays), yet can also perform readout directly in the single-spin basis. The SLQD is sensitive over a wide range of device voltages, and has been used as a compact sensor for single-electron charge detection in quantum dot arrays [17–19], as well as time-averaged single-spin measurements [20].

In this work we deploy a SLQD charge sensor in a device containing four ^{31}P donor quantum dots. We use the SLQD to perform single-shot electron spin readout in the single-spin basis on three out of the four quantum dots, achieving a maximum readout fidelity of 95%. The fourth quantum dot is found to have a tunnel rate exceeding the measurement bandwidth (300 kHz) and can not be projectively measured. We achieve an amplitude signal-to-noise ratio of 9.6 at 15-kHz measurement bandwidth, yielding $\tau_{\min} = 720$ ns. This compares favorably to previous dispersive readout measurements operating with off-chip resonators at 100–300 MHz frequencies [11–13] (respectively, $\tau_{\min} = 19\ \mu$s, 3000 μs and 8 μs).

Importantly, we find that for our donor device the detection range of the sensor is extended compared to gate-defined quantum dot architectures. Charge-sensor range is determined by the capacitive coupling between the sensor and the readout target, which in our device best matches a $1/d^{1.4\pm0.1}$ dependence as a function of sensor-qubit distance, d. Previous reports in undoped planar SiGe devices observed a $1/d^3$ dependence [21,22], and in nanowire CMOS devices a $1/d^{2.5-2.8}$ dependence was estimated based on device simulations [19]. In free space, the capacitive coupling between isolated charges scales as $1/d$, however this scaling is modified by the presence of surrounding gates and becomes $1/d^3$ for charges underneath a large metal plane [22], as is the case for gate-defined devices operated in accumulation mode [23,24]. In atomically engineered donor devices the qubit trapping potential is defined naturally by the donor, eliminating the need for additional accumulation gates and resulting in extremely low gate densities. The reduced screening in atomic precision donor devices considerably extends charge-sensor range. We estimate that our current sensor would be able to read out approximately 15 donor qubits in a linear array with high fidelity, compared to 3–4 for a sensor with similar performance in a gate-defined quantum dot device.

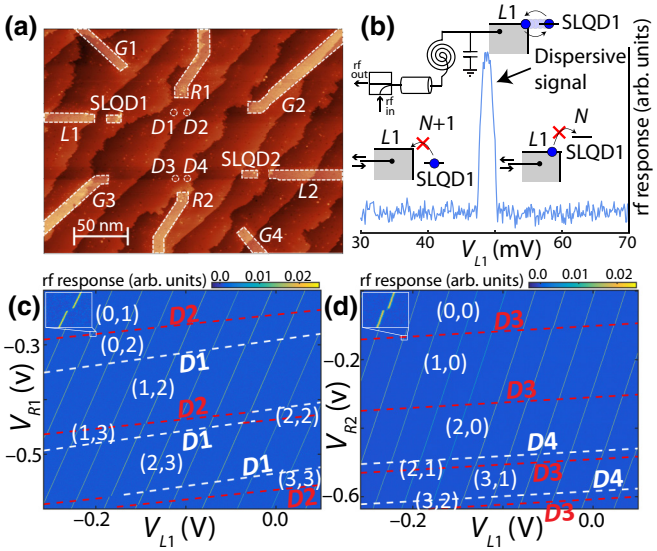

FIG. 1. **Donor-based quantum dot device with integrated SLQD charge sensors.** (a) STM image of the device and gate labels. SLQD1 is used to sense the donor quantum dots ($D1$, $D2$, $D3$, and $D4$). Based on STM images and electrically measured charging energies, we estimate the number of ^{31}P donors in each to be two for $D1$, three for $D2$, three for $D3$, and one for $D4$. Electrons are loaded onto the donors from $R1$ ($D1$, $D2$) or $R2$ ($D3$, $D4$) and onto SLQD1 from $L1$. A second SLQD (SLQD2) is not used in our experiments. (b) Schematic of SLQD charge-sensor operating principle. A quantum dot (SLQD1) tunnel coupled to an electron reservoir ($L1$) is embedded in a resonant circuit formed by a NbTiN superconducting spiral inductor, measured using standard reflectometry techniques [7]. When an ac excitation is applied to $L1$, cyclical single-electron tunneling generates quantum capacitance in the circuit when the Fermi energy in $L1$ is aligned with an available charge state of SLQD1. A change in the electrostatic environment causes the resulting Coulomb-like peaks to shift, allowing operation as a charge sensor. (c) Charge-stability diagram for $D1$ and $D2$ sweeping V_{L1} and V_{R1}. The periodic diagonal lines in the data are SLQD1 transition lines, with donor charge transitions from $D1$ and $D2$ being observed as breaks in the SLQD lines (example break shown in inset). The overlaid white dashed lines indicate $D1$ charge transitions and the red dashed lines indicate $D2$ charge transitions. (d) Charge-stability diagram for $D3$ and $D4$ sweeping V_{L1} and V_{R2}. The red dashed lines now indicate $D3$ charge transitions, and the white dashed lines $D4$ charge transitions. We note that here the $D3$ and $D4$ transition line slopes are similar; we identify the charge transitions by sweeping other gate combinations.

II. DEVICE AND SENSOR OPERATION

The four ^{31}P quantum dot device is fabricated on a silicon substrate using atomic precision hydrogen-resist lithography [25,26]. Figure 1(a) shows a STM image of the device, with sites $D1$, $D2$, $D3$, and $D4$ indicating regions where phosphorus donors are incorporated to host electron spin qubits [27]. $R1$ and $R2$ serve as electron reservoirs for ($D1$, $D2$) and ($D3$, $D4$), respectively, as well as providing electrostatic tuning of the donor potentials. $G1$ and $G2$ are electrostatic gates used for readout pulse sequences on $D1$ and $D2$, and $G3$ and $G4$ serve the same purpose for $D3$ and $D4$. SLQD1 and SLQD2 are charge sensors for determining the electron occupation of the donor dots, and to perform single-shot spin readout via spin-to-charge conversion. A schematic of the operating principle of the SLQD sensor is shown in Fig. 1(b). The sensor detects the extra quantum capacitance [7,9,10] added to the circuit when the Fermi energy of $L1$ aligns with an available

charge state on SLQD1, resulting in Coulomb-like peaks that can be used for charge sensing. We note that in this work SLQD1 is used for all measurements. Figures 1(c) and 1(d) show charge stability diagrams for the top ($D1$, $D2$) and bottom ($D3$, $D4$) pairs of donor quantum dots, respectively. The periodic diagonal lines in the data are Coulomb-like peaks from SLQD1, where donor charge transitions are observed as breaks in these lines aligned along the labelled dotted lines overlaying the data. We identify transitions from all four patterned donor quantum dots from the distinct transition line slopes, shown in Fig. 1(c) ($D1$ white dashed lines, $D2$ red dashed lines) and Fig. 1(d) ($D3$ red dashed lines, $D4$ white dashed lines). Electron numbers are assigned by fully depleting the donors of electrons, then adding an electron each time a donor transition line is crossed. We note that sweeping the reservoir lead $R1$ ($R2$) to negative voltages adds electrons to $D1$ and $D2$ ($D3$ and $D4$), in contrast to sweeping purely capacitively coupled gates, for which negative voltages remove electrons. These plots highlight the ability of SLQD1 to characterise the charge occupation of all four quantum dots.

III. SINGLE-SHOT SPIN READOUT

We next use SLQD1 to perform single-shot electron spin readout in the single-spin basis for $D1$, $D2$ and $D3$ at $B = 1.5$ T. We note that for $D4$ the tunnel rate to $R2$ exceeded our measurement bandwidth and readout could not be performed. Figure 2(a) shows a gate-gate map sweeping V_{G1} and V_{G2} over a single SLQD1 line intersecting with the first electron charge transition of $D1$. Adding an electron to $D1$ shifts the SLQD1 peak position by $V_M = 7.1$ mV (where V_M is the mutual charging voltage in terms of V_{G1}). We perform spin readout with a three-level pulse sequence consisting of a load phase to initialise a random electron spin state, followed by a read phase where the spin is projectively measured, and an empty phase to eject the electron before the next pulse repetition [4]. During the read phase a spin up state will tunnel to $R1$ followed by a spin down tunnelling back to $D1$, generating a characteristic "blip" in the charge sensor response which is absent for a spin down state. Figure 2(b) shows example spin up and spin down traces for $D1$, demonstrating single-shot readout. We calculate the spin readout fidelity by taking 5000 individual single-shot traces and find $F_M = 81\%$ (see Section 4 within the Supplemental Material for full details of the fidelity analysis [6]). The fidelity is limited by our measurement bandwidth (set to approximately 80 kHz), which is not high enough to capture the fastest tunneling events. Increasing the measurement bandwidth permits faster events at the cost of reduced SNR (which also decreases the fidelity [28]), and we find 80 kHz to give the maximum fidelity of 81%.

Figure 2(c) shows a gate-gate map at the second electron of $D2$. Here we perform D^- readout [29] due to the

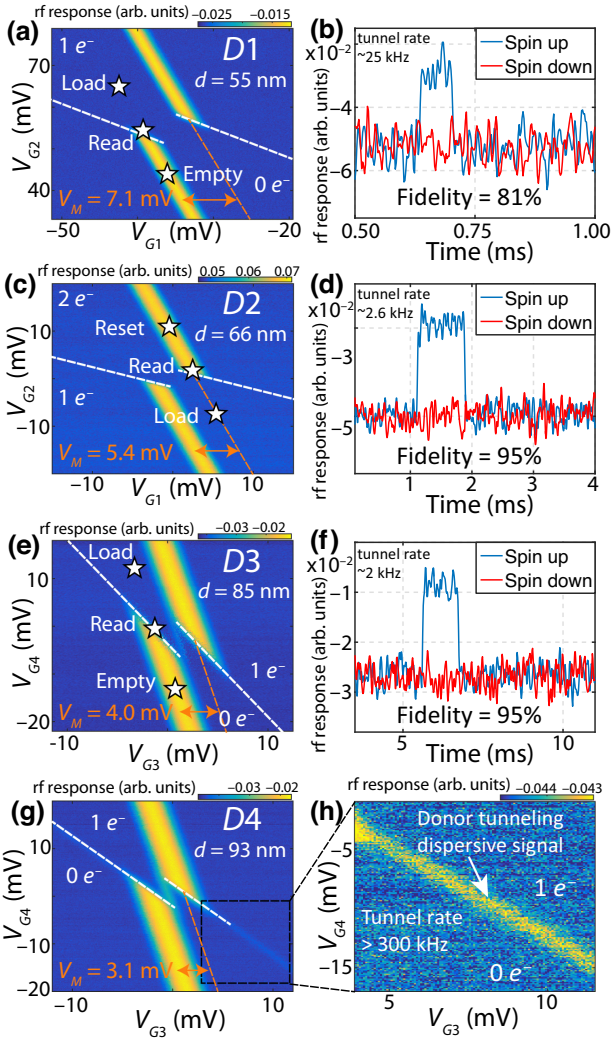

FIG. 2. **Single-shot electron spin readout on $D1$, $D2$, and $D3$ donor quantum dots.** (a) Gate-gate map showing break in SLQD1 transition line when the first electron is loaded onto $D1$. The approximate pulse positions for the readout sequence are indicated by the white stars. The read level is calibrated so that a spin-up electron can tunnel from $D1$ to $R1$, but a spin-down cannot. (b) Example single-shot readout traces showing spin-up and spin-down signals. Due to the fast tunnel rate at this transition, some of the rapid spin-up traces are not registered, leading to an average fidelity of 81%. (c) Similar gate-gate map for $D2$. Readout for $D2$ is performed at the second electron transition via the D^- charge state [29]. Here we choose the read position on the opposite side of the SLQD charge break to make spin up the high sensor level for consistency with $D1$ and $D3$. (d) Example single-shot readout traces for $D2$. (e) Gate-gate map for $D3$. (f) Example single-shot readout traces for $D3$. (g) Gate-gate map for $D4$. For this donor quantum dot, the tunnel rate between the donor and reservoir is too fast to perform single-shot spin readout. In fact, a faint signal can be observed due to cyclical driving of an electron between the $D4$ and $R2$. This implies that the tunnel rate is non-negligible compared to the rf reflectometry frequency (130 MHz). (h) Enlargement of the region from (g), highlighting the dispersive signal generated by cyclical tunneling of the $D4$ electron.

TABLE I. Summary of single-shot readout results for the four-donor-dot device.

	Donor number	Readout transition electron no.	Tunnel rate (kHz)	Distance to sensor (nm)	Sensor shift (mV)	Readout fidelity (%)	Measurement bandwidth (kHz)	Amplitude SNR	$\tau_{\min}$ (ns)
$D1$	2P	$0 \leftrightarrow 1$	~ 25	55	7.1	81	80	4.0	780
$D2$	3P	$1 \leftrightarrow 2$	~ 2.6	66	5.4	95	15	9.6	720
$D3$	3P	$0 \leftrightarrow 1$	~ 2.0	85	4.0	95	15	8.1	1020
$D4$	1P	$0 \leftrightarrow 1$	> 300	93	3.1	N/A	N/A	N/A	N/A

favorable electron tunnel rate at the second electron transition (approximately 2.6 kHz). Example single-shot traces are shown in Fig. 2(d), and taking 5000 individual traces we find a fidelity of $F_M = 95\%$ for $D2$. This fidelity is again limited in part by our finite measurement bandwidth (here 15 kHz) filtering the fastest tunneling events, as well as a relatively high electron temperature (approximately 280 mK). We note the electron temperature is not raised by the reflectometry signal applied to SLQD1 until significantly higher powers than used in our experiments. Figure 2(e) shows a gate-gate map at the first electron of $D3$. In this case electrons tunnel between $D3$ and $R2$ (rather than $R1$ as in the previous cases) during spin readout. Figure 2(f) shows corresponding example single-shot traces for $D3$, and here we find a fidelity of $F_M = 95\%$, which is limited by the same factors as $D2$.

Figure 2(g) shows a gate-gate map at the first electron transition of $D4$. Here we find that the $D4$–$R2$ tunnel rate exceeds our measurement bandwidth (approximately 300 kHz, limited by the resonator bandwidth), and we are not able to perform readout on this donor. In fact, a faint dispersive signal can be observed due to cyclical tunneling of an electron between $D4$ and $R2$ [shown in Fig. 2(h)], implying that this tunnel rate is a non-negligible fraction of the approximately 130-MHz reflectometry drive signal. Table I summarizes our spin readout results, with a maximum fidelity of 95%. By lowering the electron temperature to < 160 mK, using a higher-frequency resonant circuit and lower noise first-stage amplifier, readout of $D1$, $D2$, and $D3$ with $> 99\%$ fidelity is achievable [28–30].

IV. LONG-RANGE CHARGE SENSING

We next investigate the scaling of the SLQD1 sensor shift V_M as a function of the sensor-qubit distance d. We use the finite-element package COMSOL Multiphysics to simulate V_M for the device in Fig. 1(a) (Section 5 within the Supplemental Material [6]). Figure 3(a) plots the simulated V_M profile, with the colorscale showing the expected V_M for a qubit at the corresponding position. V_M determines the SLQD1 peak shift due to a charging event on the target qubit, and is proportional to the capacitive coupling between sensor and qubit. The white dashed contour line in Fig. 3(a) indicates the region within which V_M is large enough to shift the SLQD1 Coulomb peak from full signal (on top of the peak) to $< 1\%$ signal due to a charging event on the target qubit (the strong response threshold). Our simulations indicate that any qubit located inside the footprint of this contour would generate full *on-off* switching

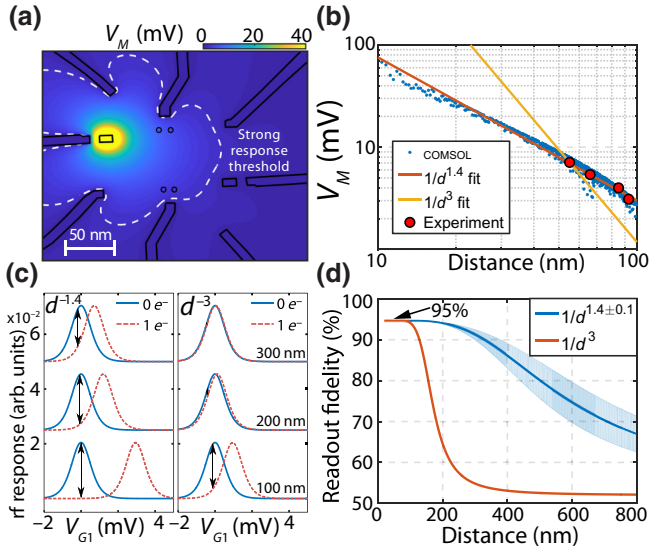

FIG. 3. **Importance of the sensor shift V_M for long-range qubit readout.** (a) COMSOL simulation of V_M for our device geometry. The dashed contour line indicates the estimated strong response regime boundary. (b) Fit to COMSOL simulated V_M values as a function of distance d from SLQD1. The simulated values (blue dots) follow a $1/d^{1.4\pm0.1}$ dependence (orange line), which match the experimental values (red circles). The yellow line is a $1/d^3$ fit (as observed in planar gate-defined devices) to the experimental data, which is inconsistent with both the simulated and measured values. (c) Comparison of readout contrast possible for 100-, 200-, and 300-nm sensor-qubit distance for $1/d^{1.4}$ scaling (left panel) and $1/d^3$ scaling (right panel). At 300 nm, the sensor peaks for the two readout charge states are almost overlapping in the $1/d^3$ case, whereas significant discrimination is still possible for $1/d^{1.4}$. (d) Estimated single-shot readout fidelity as a function of qubit distance to SLQD1. The input parameters to the fidelity calculation (tunnel rates, T_1 relaxation time, noise level) are taken from the experimentally measured values for $D3$. The blue curve is for $1/d^{1.4\pm0.1}$, with the shaded region outlining the uncertainty bounds from the fit in Fig. 3(b). The orange curve is for $1/d^3$, and exhibits a much faster roll-off in readout fidelity. Over 90% fidelity is possible out to 300 nm for $1/d^{1.4}$, compared to 130 nm for $1/d^3$.

of the sensor signal [15], and could be measured without any loss of fidelity due to the distance from the sensor.

Figure 3(b) plots the simulated V_M as a function of d (the distance from the center of SLQD1) for the device region containing the sensor and patterned donor quantum dots (shown in Fig. S4 within the Supplemental Material [6]). We note that here d is defined only by the distance to SLQD1 within the device region shown in Fig. S4 within the Supplemental Material [6], and is not a cut along one specific direction. Fitting to the simulated V_M values we find $V_M \propto d^{1.4\pm0.1}$, which is consistent with the measured data (shown by red circles). Both our experimental and simulated results are consistent with a $1/d^{1.4}$ scaling, in contrast to the $1/d^3$ scaling observed in planar gate-defined devices [21,22], indicated by the yellow curve in Fig. 3(b). Figure 3(c) highlights the significance of the capacitive scaling with d for long-range charge sensing. The left panel uses the $1/d^{1.4}$ fit from Fig. 3(b) to estimate V_M at distances of 100, 200, and 300 nm from the sensor. The solid blue and red dotted lines show the expected position of the SLQD Coulomb peak for 0 electrons and 1 electron on the target qubit at the specified distance. The shape of the sensor Coulomb peak is determined by fitting the experimental data. The vertical black arrows indicate the maximum sensor contrast for detecting the electron charge on the target. The right panel uses the $1/d^3$ fit from Fig. 3(b) to estimate V_M for 100, 200, and 300 nm from the sensor. In this case V_M decreases more rapidly with distance, and the contrast is minimal at 300 nm.

To highlight the importance of a slower roll-off for scalable quantum computing, we calculate the expected single-shot readout fidelity as a function of d for an electron spin with the same spin-dependent tunnel rates and T_1 time as $D3$ in our device. We extrapolate the fit in Fig. 3(b) to estimate V_M as a function of d, and use this to calculate the expected signal contrast. We can then calculate the SNR using the noise measured in our experiment and input this to our fidelity calculation (Section 6 within the Supplemental Material [6]). Figure 3(d) shows the result for both $1/d^{1.4\pm0.1}$ (blue curve) and $1/d^3$ (orange curve). As expected, the $1/d^3$ curve exhibits a faster roll-off in readout fidelity. For small d both red and blue curves saturate to 95% fidelity as observed in our direct experimental measurements of $D3$. We estimate that a qubit with the same properties as $D3$ could be measured with over 90% spin readout fidelity up to 300 nm from the sensor, compared to 130 nm for the $1/d^3$ scaling. We predict that the estimated 90% readout fidelity at 300 nm for our current sensor could be increased to >99% by reducing the electron temperature [29], operating the SLQD at higher frequencies and using a lower noise first-stage amplifier [30].

With a 300-nm sensor range, the small size of donor qubits means that a single sensor has the potential to serve a large number of qubits. A leading proposal for a donor-based surface-code architecture uses a donor separation distance of 30 nm [1]. Linear arrays are the current experimental state of the art in semiconductor spin qubits; for a linear array of donor qubits with an interqubit separation of 30 nm, our results suggest that we would be able to read out $\lesssim 20$ donor qubits with high fidelity with SLQD1 placed in the center of the array. To verify the predicted qubit number that could be sensed we directly simulate

TABLE II. Improvement in estimated qubits per sensor compared to previous gate-based readout results.

Reference	τ_{min}	Sensor type	Device type	Max spin readout fidelity	Readout basis	Estimated capacitive scaling	Estimated qubits per sensor
Pakkiam *et al.*, (2018) [11]	19 μs	Direct dispersive	Precision donor	83%	Singlet/triplet	$1/d^{1.4}$	1
West *et al.*, (2019) [12]	3000 μs	Direct dispersive	Planar MOS	73%	Singlet/triplet	$1/d^3$	1
Zheng *et al.*, (2019) [14]	170 ns	Direct dispersive	SiGe	98%	Singlet/triplet	$1/d^3$	1
Urdampiletta *et al.*, (2019) [13]	8 μs	Latched SLQD	Nanowire MOS	98%	Singlet/triplet	$1/d^{2.5-2.8}$	1-3
Chanrion *et al.*, (2020) [17]	21 μs	SLQD	Nanowire MOS	N/A	N/A	$1/d^{2.5-2.8}$	3
Ansaloni *et al.*, (2020) [18]	17 μs	SLQD	Nanowire MOS	N/A	N/A	$1/d^{2.5-2.8}$	3
Cirano-Tejel *et al.*, (2020) [20]	50 μs	SLQD	Nanowire MOS	N/A	Single spin	$1/d^{2.5-2.8}$	3
Duan *et al*, (2020) [19]	9 μs	SLQD	Nanowire MOS	N/A	N/A	$1/d^{2.5-2.8}$	3
Hogg *et al.*, (this work)	**720 ns**	**SLQD**	**Precision donor**	**95%**	**Single spin**	$\mathbf{1/d^{1.4}}$	**15**

a realistic linear array of donor qubits (see Section 7 within the Supplemental Material [6]), from which we estimate that sensing 14–16 qubits is feasible using our current SLQD sensor. For the geometry and scaling expected in an accumulation-mode gate-defined device ($1/d^3$, assuming a qubit separation of 80 nm and sensor range of 130 nm), the equivalent number is $\lesssim 4$. This is consistent with current experimental demonstrations having 3–4 qubits per sensor [21,31]. Table II compares our result to recently reported gate-based sensing literature, demonstrating the significant improvement in the number of possible qubits per sensor in a linear array (see Section 6 within the Supplemental Material for further details [6]).

Given the extremely long T_1 relaxation times in donor qubits (we measure approximately 11 s for $D3$ at 1.5 tesla, and up to 30 s has been demonstrated [32]) and recent advances navigating charge states in large qubit arrays [31,33], 15 qubits similar to $D3$ could be measured sequentially by the same sensor within the T_1 relaxation time. For our present sensor, sequential measurements would be too slow for quantum error-correction cycles; however, for an optimized sensor 15 qubits could be measured within the measured T_2^* times of donor electron spin qubits (270 μs in isotopically purified silicon [34]). We note that reducing the electron temperature would narrow the SLQD Coulomb peaks, increasing the charge detection signal for small V_M shifts and further extending the sensor range (and thus the number of qubits measured) beyond our current estimate. We also note that donor qubits can be placed significantly closer than 30 nm using atomic precision lithography. For an architecture of tunnel coupled donors (typically separated by 10–15 nm), a single optimized SLQD sensor could conceivably serve a linear array of 50–100 donor qubits.

V. CONCLUSION

In conclusion, we have demonstrated single-shot electron spin readout in the single-spin basis using a SLQD charge sensor. In a device with four ^{31}P donor quantum dots we performed single-shot readout on three of the four quantum dots with fidelities of 81%, 95%, and 95%. We note that these fidelities can be significantly improved in future experiments; fidelities of 99.8% (above the fault-tolerant threshold) have been achieved for single-spin readout using SETs [32], which should be achievable using our SLQD approach. Readout in the two-spin singlet-triplet basis is also possible using our flexible sensor, for which fidelities $> 98\%$ have been demonstrated in multiple experiments [13,14,35].

We also found that due to the low gate density in our atomic precision donor device, the capacitive coupling between sensor and qubits is consistent with a $1/d^{1.4}$ dependence compared to the $1/d^{2.5-3.0}$ dependence observed in gate-defined devices that accumulate qubit electrons below metallic gates. As a consequence, charge-sensor range is significantly extended in our device compared to such gate-defined devices. Because of this extended range and the small size of donor qubits, we estimate that our current sensor could projectively measure approximately 15 donor spin qubits in a linear array. Our results highlight the prospect of large-scale quantum computing architectures with significantly reduced sensor densities in atom-scale spin qubits.

VI. METHODS

Device fabrication: The device is fabricated on a p-type natural Si substrate (1–10Ω cm) using a STM to perform atomic precision hydrogen-resist lithography [36]. A fully terminated H:Si(2×1) reconstructed surface is prepared in an ultrahigh vacuum chamber (approximately 10^{-12} mbar). The STM tip is used to selectively remove hydrogen atoms to create a lithographic mask, which defines the device. The regions of desorbed hydrogen are n doped with ^{31}P by introducing a gaseous PH_3 precursor into the chamber, which adsorbs to the silicon surface only where the hydrogen has been removed. Subsequent annealing (at 350 °C) incorporates the ^{31}P atoms into the silicon crystal. Removing only a few hydrogen atoms allows the fabrication of atomic scale donor quantum dots. The device is then encapsulated with 50 nm of silicon, grown by molecular-beam epitaxy. The resulting structure consists of the qubit device embedded in crystalline silicon. The device is then removed from the STM chamber and contacted electrically with aluminium Ohmic contacts through etched via holes.

Measurement details: The device chip is bonded to a PCB to deliver high-frequency signals and dc voltages then mounted to the cold finger of a dilution refrigerator with approximately 80 mK base temperature. We use a NbTiN superconducting spiral inductor for reflectometry measurements, with a resonance frequency of approximately 130 MHz and a loaded quality factor of approximately 400 when bonded to $L1$. An ac signal is first attenuated before being applied to $L1$, with the reflected signal being separated to the output chain using a directional coupler, before amplification (at 4 K using a CITLF3 low-noise amplifier, and at room temperature with a Pasternack PE15A1012), demodulation (Polyphase AD0105B) and acquisition with a digitiser card (NI-USB-6363). Spin readout pulse sequences are generated by an AWG (Tektronix AWG5204).

ACKNOWLEDGMENTS

This research was conducted by the Australian Research Council Centre of Excellence for Quantum Computation and Communication Technology (Project No. CE170100012) and Silicon Quantum Computing Pty Ltd. M.Y.S. acknowledges an Australian Research Council

Laureate Fellowship. The device was fabricated in part at the NSW node of the Australian National Fabrication Facility (ANFF).

Note added.—Recently, we became aware of another work demonstrating single-shot single-spin readout using a SLQD [37], however readout of only one spin was performed.

AUTHOR CONTRIBUTIONS

M.R.H. conceived the project and designed the device with input from P.P. M.R.H. fabricated the device with assistance from Y.C. M.R.H. performed the measurements and data analysis with input from M.G.H. A.V.T. designed and fabricated the superconducting inductor used for reflectometry. S.K.G. calculated the spin readout fidelities. G.K.G. assisted with the spin relaxation measurements. P.P. and M.R.H. performed the COMSOL modeling. M.R.H., S.K.G., and M.Y.S. wrote the manuscript with input from M.G.H. M.G.H. and M.Y.S. supervised the project.

AUTHOR INFORMATION

Correspondence and requests for materials should be addressed to M.Y.S. (michelle.simmons@unsw.edu.au).

COMPETING FINANCIAL INTERESTS

M.Y.S. is a director of the company Silicon Quantum Computing Pty Ltd. All other authors declare no competing financial interests.

[1] C. D. Hill, E. Peretz, S. J. Hile, M. G. House, M. Fuechsle, S. Rogge, M. Y. Simmons, and L. C. Hollenberg, A surface code quantum computer in silicon, Sci. Adv. **1**, 1 (2015).

[2] M. Veldhorst, H. G. J. Eenink, C. H. Yang, and A. S. Dzurak, Silicon CMOS architecture for a spin-based quantum computer, Nat. Commun. **8**, 1766 (2017).

[3] J. M. Elzerman, R. Hanson, L. H. Willems van Beveren, B. Witkamp, L. M. K. Vandersypen, and L. P. Kouwenhoven, Single-shot read-out of an individual electron spin in a quantum dot, Nature **430**, 431 (2004).

[4] A. Morello, J. J. Pla, F. A. Zwanenburg, K. W. Chan, K. Y. Tan, H. Huebl, M. Möttönen, C. D. Nugroho, C. Yang, J. A. van Donkelaar, A. D. C. Alves, D. N. Jamieson, C. C. Escott, L. C. L. Hollenberg, R. G. Clark, and A. S. Dzurak, Single-shot readout of an electron spin in silicon, Nature **467**, 687 (2010).

[5] D. Keith, M. G. House, M. B. Donnelly, T. F. Watson, B. Weber, and M. Y. Simmons, Single-Shot Spin Readout in Semiconductors Near the Shot-Noise Sensitivity limit, Phys. Rev. X **9**, 041003 (2019).

[6] See Supplemental Material at http://link.aps.org/supplemental/10.1103/PRXQuantum.4.010319 for details regarding optimiziation of the charge sensor, readout fidelity analysis, and further details of COMSOL simulations, which includes Refs. [38–43].

[7] K. D. Petersson, C. G. Smith, D. Anderson, P. Atkinson, G. A. C. Jones, and D. A. Ritchie, Charge and spin state readout of a double quantum dot coupled to a resonator, Nano Lett. **10**, 2789 (2010).

[8] J. I. Colless, A. C. Mahoney, J. M. Hornibrook, A. C. Doherty, H. Lu, A. C. Gossard, and D. J. Reilly, Dispersive Readout of a Few-Electron Double Quantum Dot with Fast rf Gate Sensors, Phys. Rev. Lett. **110**, 046805 (2013).

[9] M. G. House, T. Kobayashi, B. Weber, S. J. Hile, T. F. Watson, J. van der Heijden, S. Rogge, and M. Y. Simmons, Radio frequency measurements of tunnel couplings and singlet–triplet spin states in Si:P quantum dots, Nat. Commun. **6**, 8848 (2015).

[10] M. F. Gonzalez-Zalba, S. Barraud, A. J. Ferguson, and A. C. Betz, Probing the limits of gate-based charge sensing, Nat. Commun. **6**, 6084 (2015).

[11] P. Pakkiam, A. V. Timofeev, M. G. House, M. R. Hogg, T. Kobayashi, M. Koch, S. Rogge, and M. Y. Simmons, Single-Shot Single-Gate rf Spin Readout in Silicon, Phys. Rev. X 8, 041032 (2018). ArXiv:1809.01802,.

[12] A. West, B. Hensen, A. Jouan, T. Tanttu, C. H. Yang, A. Rossi, M. F. Gonzalez-Zalba, F. Hudson, A. Morello, D. J. Reilly, and A. S. Dzurak, Gate-based single-shot readout of spins in silicon, Nat. Nanotechnol. 14, 437 (2019). ArXiv:1809.01864,.

[13] M. Urdampilleta, D. J. Niegemann, E. Chanrion, B. Jadot, C. Spence, P.-A. Mortemousque, C. Bäuerle, L. Hutin, B. Bertrand, S. Barraud, R. Maurand, M. Sanquer, X. Jehl, S. De Franceschi, M. Vinet, and T. Meunier, Gate-based high fidelity spin readout in a CMOS device, Nat. Nanotechnol. **14**, 737 (2019).

[14] G. Zheng, N. Samkharadze, M. L. Noordam, N. Kalhor, D. Brousse, A. Sammak, G. Scappucci, and L. M. Vandersypen, Rapid gate-based spin read-out in silicon using an on-chip resonator, Nat. Nanotechnol. **14**, 742 (2019).

[15] F. Borjans, X. Mi, and J. R. Petta, Spin Digitizer for High-Fidelity Readout of a Cavity-Coupled Silicon Triple Quantum Dot, Phys. Rev. Appl. **15**, 044052 (2021).

[16] M. G. House, I. Bartlett, P. Pakkiam, M. Koch, E. Peretz, J. van der Heijden, T. Kobayashi, S. Rogge, and M. Y. Simmons, High-Sensitivity Charge Detection with a Single-Lead Quantum Dot for Scalable Quantum Computation, Phys. Rev. Appl. **6**, 044016 (2016).

[17] E. Chanrion, D. J. Niegemann, B. Bertrand, C. Spence, B. Jadot, J. Li, P.-A. Mortemousque, L. Hutin, R. Maurand, X. Jehl, M. Sanquer, S. De Franceschi, C. Bäuerle, F. Balestro, Y.-M. Niquet, M. Vinet, T. Meunier, and M. Urdampilleta, Charge Detection in an Array of CMOS Quantum Dots, Phys. Rev. Appl. **14**, 024066 (2020).

[18] F. Ansaloni, A. Chatterjee, H. Bohuslavskyi, B. Bertrand, L. Hutin, M. Vinet, and F. Kuemmeth, Single-electron operations in a foundry-fabricated array of quantum dots, Nat. Commun. **11**, 6399 (2020).

[19] J. Duan, M. A. Fogarty, J. Williams, L. Hutin, M. Vinet, and J. J. L. Morton, Remote capacitive sensing in two-dimensional quantum-dot arrays, Nano Lett. **20**, 7123 (2020). pMID: 32946244,.

[20] V. N. Ciriano-Tejel, M. A. Fogarty, S. Schaal, L. Hutin, B. Bertrand, L. Ibberson, M. F. Gonzalez-Zalba, J. Li, Y. M. Niquet, M. Vinet, and J. J. L. Morton, Spin Readout of a CMOS Quantum Dot by Gate Reflectometry and Spin-Dependent Tunneling, PRX Quantum **2**, 010353 (2021).

[21] D. M. Zajac, T. M. Hazard, X. Mi, E. Nielsen, and J. R. Petta, Scalable Gate Architecture for a One-Dimensional Array of Semiconductor Spin Qubits, Phys. Rev. Appl. **6**, 054013 (2016).

[22] S. F. Neyens, E. R. MacQuarrie, J. P. Dodson, J. Corrigan, N. Holman, B. Thorgrimsson, M. Palma, T. McJunkin, L. F. Edge, M. Friesen, S. N. Coppersmith, and M. A. Eriksson, Measurements of Capacitive Coupling Within a Quadruple-Quantum-Dot Array, Phys. Rev. Appl. **12**, 064049 (2019).

[23] M. G. Borselli, K. Eng, R. S. Ross, T. M. Hazard, K. S. Holabird, B. Huang, A. A. Kiselev, P. W. Deelman, L. D. Warren, I. Milosavljevic, A. E. Schmitz, M. Sokolich, M. F. Gyure, and A. T. Hunter, Undoped accumulation-mode Si/SiGe quantum dots, Nanotechnology **26**, 375202 (2015).

[24] W. H. Lim, F. A. Zwanenburg, H. Huebl, M. Möttönen, K. W. Chan, A. Morello, and A. S. Dzurak, Observation of the single-electron regime in a highly tunable silicon quantum dot, Appl. Phys. Lett. **95**, 242102 (2009).

[25] M. Simmons, F. Ruess, K. Goh, T. Hallam, S. Schofield, L. Oberbeck, N. Curson, A. Hamilton, M. Butcher, R. Clark, and T. Reusch, Scanning probe microscopy for silicon device fabrication, Mol. Simul. **31**, 505 (2005).

[26] M. Fuechsle, J. A. Miwa, S. Mahapatra, H. Ryu, S. Lee, O. Warschkow, L. C. L. Hollenberg, G. Klimeck, and M. Y. Simmons, A single-atom transistor, Nat. Nanotechnol. **7**, 242 (2012).

[27] Y. He, S. K. Gorman, D. Keith, L. Kranz, J. G. Keizer, and M. Y. Simmons, A two-qubit gate between phosphorus donor electrons in silicon, Nature **571**, 371 (2019).

[28] D. Keith, S. K. Gorman, L. Kranz, Y. He, J. G. Keizer, M. A. Broome, and M. Y. Simmons, Benchmarking high fidelity single-shot readout of semiconductor qubits, New J. Phys. **21**, 063011 (2019).

[29] T. F. Watson, B. Weber, M. G. House, H. Büch, and M. Y. Simmons, High-Fidelity Rapid Initialization and Read-Out of an Electron Spin via the Single Donor D^- Charge State, Phys. Rev. Lett. **115**, 166806 (2015).

[30] S. Schaal, I. Ahmed, J. A. Haigh, L. Hutin, B. Bertrand, S. Barraud, M. Vinet, C.-M. Lee, N. Stelmashenko, J. W. A. Robinson, J. Y. Qiu, S. Hacohen-Gourgy, I. Siddiqi, M. F. Gonzalez-Zalba, and J. J. L. Morton, Fast Gate-Based Readout of Silicon Quantum Dots using Josephson Parametric Amplification, Phys. Rev. Lett. **124**, 067701 (2020).

[31] C. Volk, A. M. J. Zwerver, U. Mukhopadhyay, P. T. Eendebak, C. J. van Diepen, J. P. Dehollain, T. Hensgens, T. Fujita, C. Reichl, W. Wegscheider, and L. M. K. Vandersypen, Loading a quantum-dot based "qubyte" register, npj Quantum Inf. **5**, 29 (2019).

[32] T. F. Watson, B. Weber, Y.-L. Hsueh, L. C. L. Hollenberg, R. Rahman, and M. Y. Simmons, Atomically engineered electron spin lifetimes of 30 s in silicon, Sci. Adv. **3**, e1602811 (2017).

[33] A. R. Mills, D. M. Zajac, M. J. Gullans, F. J. Schupp, T. M. Hazard, and J. R. Petta, Shuttling a single charge across a one-dimensional array of silicon quantum dots, Nat. Commun. **10**, 1063 (2019).

[34] J. T. Muhonen, J. P. Dehollain, A. Laucht, F. E. Hudson, R. Kalra, T. Sekiguchi, K. M. Itoh, D. N. Jamieson, J. C. McCallum, A. S. Dzurak, and A. Morello, Storing quantum information for 30 seconds in a nanoelectronic device, Nat. Nanotechnol. **9**, 986 (2014).

[35] P. Harvey-Collard, B. D'Anjou, M. Rudolph, N. T. Jacobson, J. Dominguez, G. A. TenEyck, J. R. Wendt, T. Pluym, M. P. Lilly, W. A. Coish, M. Pioro-Ladrière, and M. S. Carroll, High-Fidelity Single-Shot Readout for a Spin Qubit via an Enhanced Latching Mechanism, Phys. Rev. X **8**, 021046 (2018).

[36] M. Fuechsle, S. Mahapatra, F. A. Zwanenburg, M. Friesen, M. A. Eriksson, and M. Y. Simmons, Spectroscopy of few-electron single-crystal silicon quantum dots, Nat. Nanotechnol. **5**, 502 (2010).

[37] G. A. Oakes, V. N. Ciriano-Tejel, D. Wise, M. A. Fogarty, T. Lundberg, C. Lainé, S. Schaal, F. Martins, D. J. Ibberson, L. Hutin, B. Bertrand, N. Stelmashenko, J. A. W. Robinson, L. Ibberson, A. Hashim, I. Siddiqi, A. Lee, M. Vinet, C. G. Smith, J. J. L. Morton, and M. F. Gonzalez-Zalba, Fast high-fidelity single-shot readout of spins in silicon using a single-electron box (2022), ArXiv:2203.06608.

[38] I. Ahmed, J. A. Haigh, S. Schaal, S. Barraud, Y. Zhu, C.-m. Lee, M. Amado, J. W. A. Robinson, A. Rossi, J. J. L. Morton, and M. F. Gonzalez-Zalba, Radio-Frequency Capacitive Gate-Based Sensing, Phys. Rev. Appl. **10**, 014018 (2018).

[39] J. Stehlik, Y.-Y. Liu, C. M. Quintana, C. Eichler, T. R. Hartke, and J. R. Petta, Fast Charge Sensing of a Cavity-Coupled Double Quantum Dot using a Josephson Parametric Amplifier, Phys. Rev. Appl. **4**, 014018 (2015).

[40] R. J. Schoelkopf, P. Wahlgren, A. A. Kozhevnikov, P. Delsing, and D. E. Prober, The radio-frequency single-electron transistor (rf-SET): A fast and ultrasensitive electrometer, Science **280**, 1238 (1998).

[41] R. Rahman, C. J. Wellard, F. R. Bradbury, M. Prada, J. H. Cole, G. Klimeck, and L. C. L. Hollenberg, High Precision Quantum Control of Single Donor Spins in Silicon, Phys. Rev. Lett. **99**, 036403 (2007).

[42] A. Laucht, J. T. Muhonen, F. A. Mohiyaddin, R. Kalra, J. P. Dehollain, S. Freer, F. E. Hudson, M. Veldhorst, R. Rahman, G. Klimeck, K. M. Itoh, D. N. Jamieson, J. C. McCallum, A. S. Dzurak, and A. Morello, Electrically controlling single-spin qubits in a continuous microwave field, Sci. Adv. **1**, e1500022 (2015).

[43] B. Weber, S. Mahapatra, H. Ryu, S. Lee, A. Fuhrer, T. C. G. Reusch, D. L. Thompson, W. C. T. Lee, G. Klimeck, L. C. L. Hollenberg, and M. Y. Simmons, Ohm's law survives to the atomic scale, Science **335**, 64 (2012).